Available online at www.sciencedirect.com
SCIENCE DIRECT®
Physica B 338 (2003) 8–15
PHYSICA B
www.elsevier.com/locate/physb

Micromechanics-based determination of effective elastic properties of polymer bonded explosives

Biswajit Banerjee*, Daniel O. Adams

Department of Mechanical Engineering, University of Utah, 50 S Central Campus Dr., Salt Lake City, UT 84112, USA

Abstract

Polymer bonded explosives are particulate composites containing a high volume fraction of stiff elastic explosive particles in a compliant viscoelastic binder. Since the volume fraction of particles can be greater than 0.9 and the modulus contrast greater than 20 000, rigorous bounds on the elastic moduli of the composite are an order of magnitude different from experimentally determined values. Analytical solutions are also observed to provide inaccurate estimates of effective elastic properties. Direct finite element approximations of effective properties require large computational resources because of the complexity of the microstructure of these composites. An alternative approach, the recursive cells method (RCM) is also explored in this work. Results show that the degree of discretization and the microstructures used in finite element models of PBXs can significantly affect the estimated Young's moduli.

PACS: 46.65.+g; 81.05.Qk; 81.40.Jj; 61.41.+e; 61.43.−j; 61.43.Bn; 61.43.Hv; 62.20.Dc

Keywords: Effective properties; High volume fraction; High modulus contrast

1. Introduction

Mechanical properties of polymer bonded explosives (PBXs) have traditionally been determined experimentally. However, the hazardous nature of these materials makes mechanical testing expensive. With improvement in computational power, numerical determination of mechanical properties of PBXs has become feasible. Elastic properties of a composite can be obtained using micromechanics-based methods if the elastic properties of the components are known from molecular dynamics simulations. In this work, rigorous bounds, effective medium approximations and finite element approximations of elastic properties are explored. A less computationally intensive approach, called the recursive cells method (RCM) is also investigated. The properties predicted by these approaches are compared with experimental data for PBX 9501.

2. PBX materials and PBX 9501

PBXs are particulate composites composed of explosive particles and a rubbery binder. PBX 9501 contains 92% by volume of HMX (high-melting explosive) particles and 8% by volume of binder. The HMX particles are monoclinic and linear elastic. The experimentally determined value

*Corresponding author. Fax: 801-585-9826.
E-mail address: banerjee@eng.utah.edu (B. Banerjee).

0921-4526/$ - see front matter
doi:10.1016/S0921-4526(03)00451-4

of Young's modulus of HMX is around 15.3 GPa [1] while that from molecular dynamics (MD) simulations is around 17.7 GPa [2]. The Poisson's ratio from experiments is 0.32 and that from MD simulations is 0.21. The binder is a 1:1 mixture of the rubber Estane 5703 and a plasticizer (BDNPA/F). The mechanical behavior of the binder is strain rate and temperature dependent. As a result, the response of PBX 9501 also depends on strain rate and temperature. At or near room temperature and at low strain rate, the Young's modulus of the binder is around 0.7 MPa and the Poisson's ratio is 0.49 [3,4]. The Young's modulus of PBX 9501 under these conditions is around 1 GPa and the Poisson's ratio is 0.35. The modulus contrast between HMX and the binder is 15 000–20 000 under these conditions.

3. Micromechanics approaches

3.1. Third-order bounds

Third-order bounds [5] on the effective properties of two-component polydisperse particulate composites can be written as

$$K_c^U = \langle K\rangle - \frac{3f_p f_b (K_p - K_b)^2}{3\widetilde{\langle K\rangle} + 4\langle G\rangle_\zeta}, \tag{1}$$

$$G_c^U = \langle G\rangle - \frac{6f_p f_b (G_p - G_b)^2}{6\widetilde{\langle G\rangle} + \Theta}, \tag{2}$$

$$1/K_c^L = \langle 1/K\rangle - \frac{4f_p f_b (1/K_p - 1/K_b)^2}{4\widetilde{\langle 1/K\rangle} + 3\langle 1/G\rangle_\zeta}, \tag{3}$$

$$1/G_c^L = \langle 1/G\rangle - \frac{f_p f_b (1/G_p - 1/G_b)^2}{\widetilde{\langle 1/G\rangle} + 6\Xi}, \tag{4}$$

where f is a volume fraction, K is a bulk modulus and G is a shear modulus. The subscripts p, b, and c denote the particle, binder, and composite, respectively. The superscripts U and L denote the upper and lower bounds, respectively. For any quantity a, $\langle a\rangle = a_p f_p + a_b f_b$, $\widetilde{\langle a\rangle} = a_p f_b + a_b f_p$, $\langle a\rangle_\zeta = a_p\zeta_p + a_b\zeta_b$, and $\langle a\rangle_\eta = a_p\eta_p + a_b\eta_b$. The quantities ζ_p and η_p for polydisperse composites are given by $\zeta_p = 1 - \zeta_b = 0.5 f_p$ and $\eta_p = 1 - \eta_b = 0.5 f_p$. Also, $\Xi = (10\langle K\rangle^2\langle 1/K\rangle_\zeta + 5\langle G\rangle\langle 3G+2K\rangle\langle 1/G\rangle_\zeta + \langle 3K+G\rangle^2\langle 1/G\rangle_\eta)/\langle 9K+8G\rangle^2$ and $\Theta = (10\langle G\rangle^2\langle K\rangle_\zeta + 5\langle G\rangle\langle 3G+2K\rangle\langle G\rangle_\zeta + \langle 3K+G\rangle^2\langle G\rangle_\eta/\langle K+2G\rangle^2$.

3.2. Differential effective medium approximation

Effective elastic moduli can be calculated using the differential effective medium approximation (DEM) [6] from the equations

$$(1-f_p)\frac{dK_c}{df_p} = (K_p - K_c)\left(\frac{K_c + 4/3G_c}{K_p + 4/3G_c}\right), \tag{5}$$

$$(1-f_p)\frac{dG_c}{df_p} = (G_p - G_c)\left(\frac{G_c + \varphi_c}{K_p + \varphi_c}\right), \tag{6}$$

where the same symbols are used as in Eqs. (1)–(4) and $\varphi_c = G_c/6 \times (9K_c + 8G_c)/(K_c + 2G_c)$.

3.3. Finite element approximation

Finite element (FEM) approximations of two-dimensional effective elastic moduli of a composite can be obtained by determining the average stresses and strains in a representative volume element (RVE) under normal and shear displacement boundary conditions using Eq. (7)

$$\begin{bmatrix}\langle\varepsilon_{11}\rangle\\ \langle\varepsilon_{22}\rangle\\ \langle\gamma_{12}\rangle\end{bmatrix} = \begin{bmatrix}1/E_{11}^c & -\nu_{21}^c/E_{11}^c & 0\\ -\nu_{12}^c/E_{22}^c & 1/E_{22}^c & 0\\ 0 & 0 & 1/G_{12}^c\end{bmatrix}\begin{bmatrix}\langle\sigma_{11}\rangle\\ \langle\sigma_{22}\rangle\\ \langle\tau_{12}\rangle\end{bmatrix}, \tag{7}$$

where $\langle\varepsilon_{ii}\rangle$, $\langle\sigma_{ii}\rangle$ are the volume averaged normal strains and stresses; $\langle\gamma_{12}\rangle$, $\langle\tau_{12}\rangle$ are the volume averaged shear strain and stress; E_{ii}^c, G_{12}^c, ν_{ij}^c are the two-dimensional effective Young's moduli, shear modulus, and Poisson's ratios, respectively. These two-dimensional moduli are converted to three-dimensional moduli using the relations $\nu_{eff}^{3D} = \nu_{eff}^{2D}/(1+\nu_{eff}^{2D})$ and $E_{eff}^{3D} = E_{eff}^{2D}[1-(\nu_{eff}^{3D})^2]$.

3.4. Recursive cells method

In the recursive cells method (RCM) the RVE is divided into a regular grid of subcells. Instead of

determining the effective properties of the whole RVE at a time, smaller blocks of subcells are homogenized and the procedure is repeated recursively until the effective property of the RVE is obtained as shown in Fig. 1. This approach is similar to real-space renormalization techniques used to predict effective conductivities of random composites [7]. The current implementation of RCM uses finite element analyses to determine the effective properties of a block of subcells.

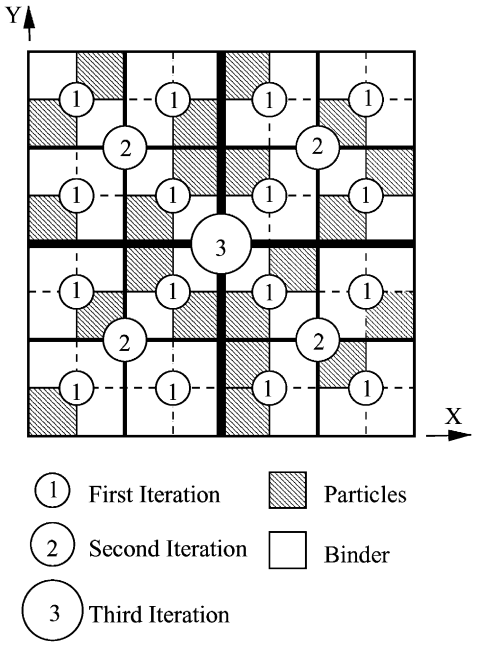

Fig. 1. Schematic of the recursive cells method.

4. Results and discussion

Third-order bounds on the Young's modulus of PBX 9501 computed using Eqs. (1)–(4) are an order of magnitude different from the experimentally determined value. A better estimate is obtained from the DEM approximation—around $\frac{1}{5}$th the experimental Young's modulus of PBX 9501. Fig. 2 shows 10 two-dimensional RVEs with particle volume fractions from 0.1 to 0.92, circular particles, and no particle–particle contact, that have been used for FEM and RCM calculations.

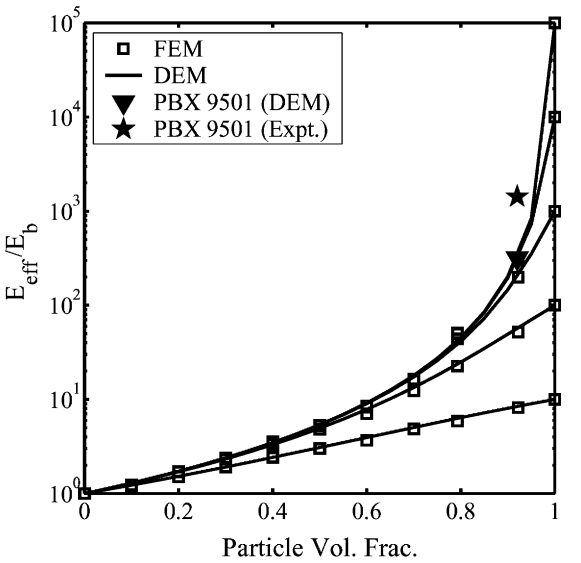

Fig. 3. Comparison of DEM and FEM estimates of Young's modulus.

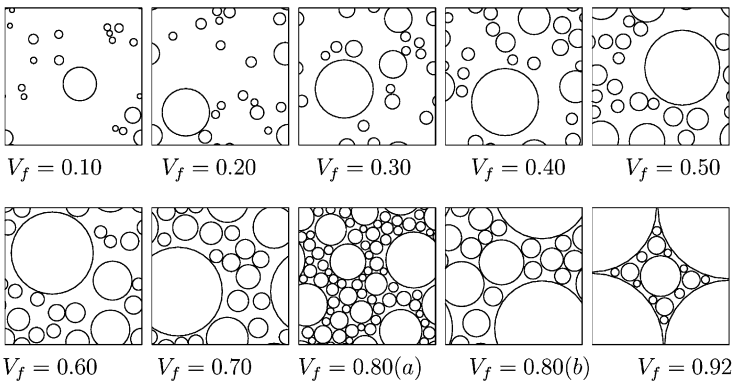

Fig. 2. RVEs containing 10–92% circular particles.

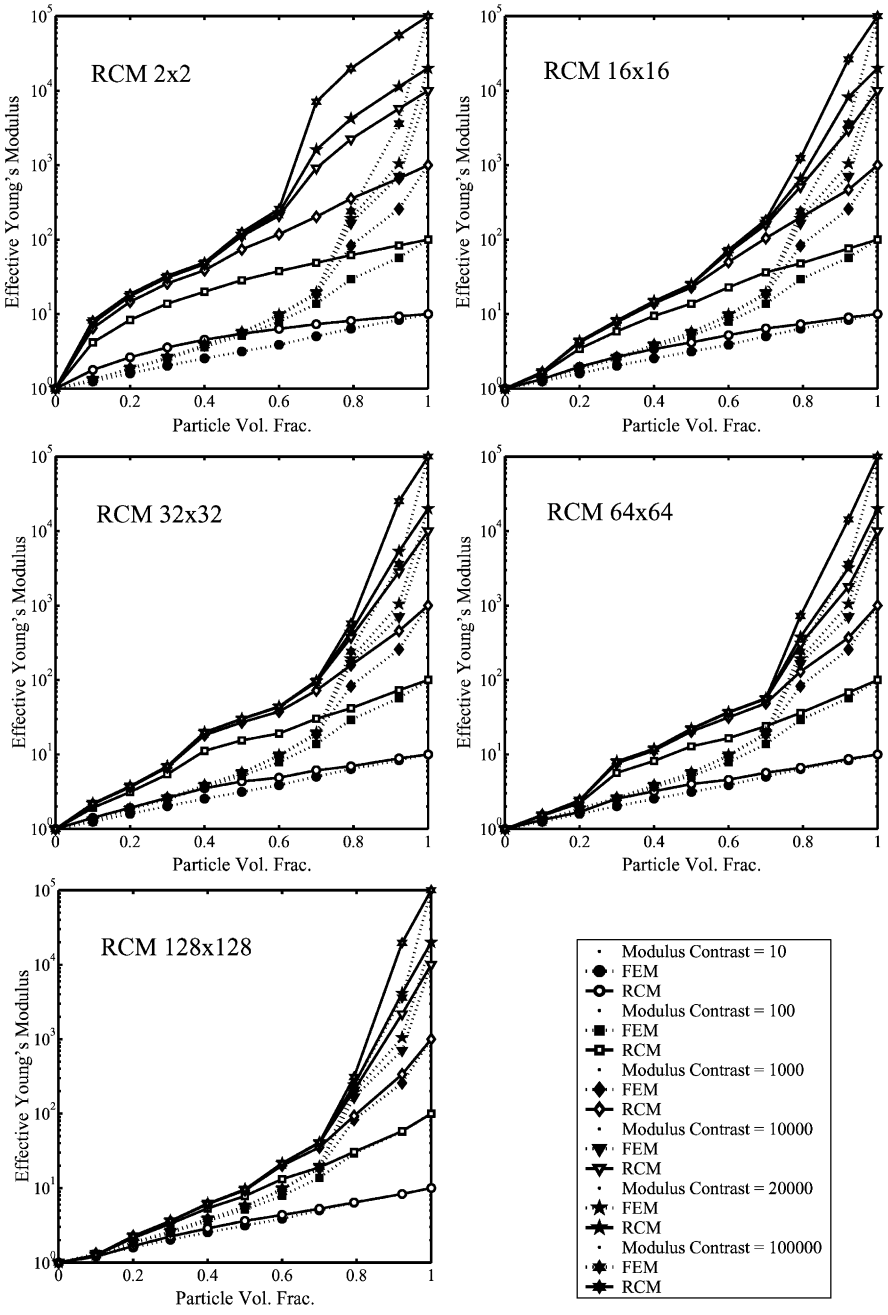

Fig. 4. Comparisons of FEM and RCM estimates of Young's modulus. The larger RVE (a) has been used for $V_f = 0.80$.

Fig. 3 shows the effective Young's modulus of these RVEs calculated by FEM, using about 70 000 six-noded triangular elements, compared to DEM predictions. The DEM and FEM predictions match closely. However, the FEM estimate for a volume fraction of 0.92 is only 20% of the experimental Young's modulus of PBX 9501. An increased estimate of the Young's modulus

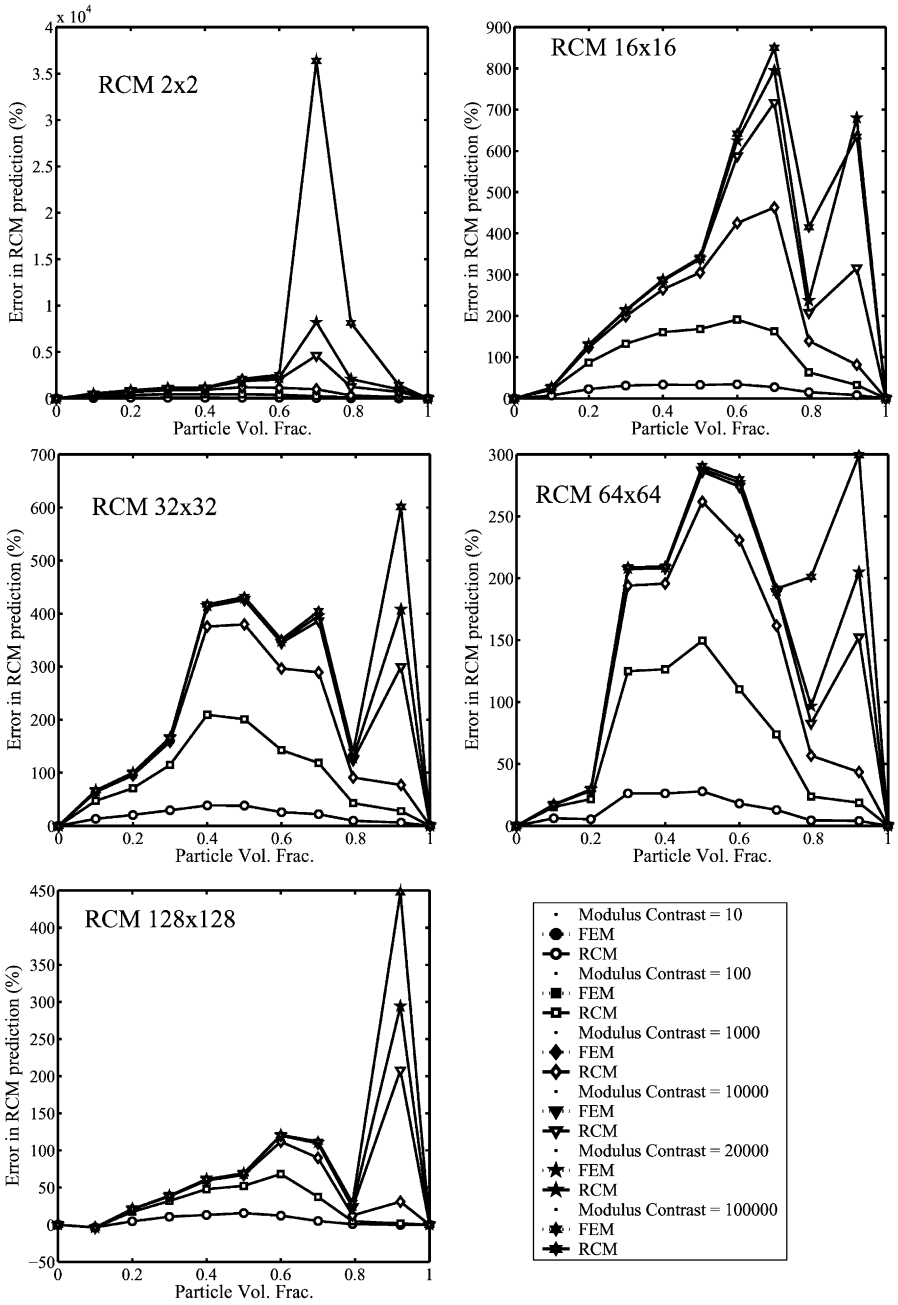

Fig. 5. Error in RCM estimates of Young's modulus with respect to FEM estimates. The larger RVE (a) has been used for $V_f = 0.80$.

requires that stress-bridging be incorporated in a RVE that models PBX 9501. Stress-bridging can be simulated by approximating the circular particles by dividing each RVE into a regular grid containing 256×256 subcells/elements. From the stress-bridging model containing 92% particles, the FEM estimate of the Young's modulus of PBX 9501 is 800 MPa. This value of modulus is only

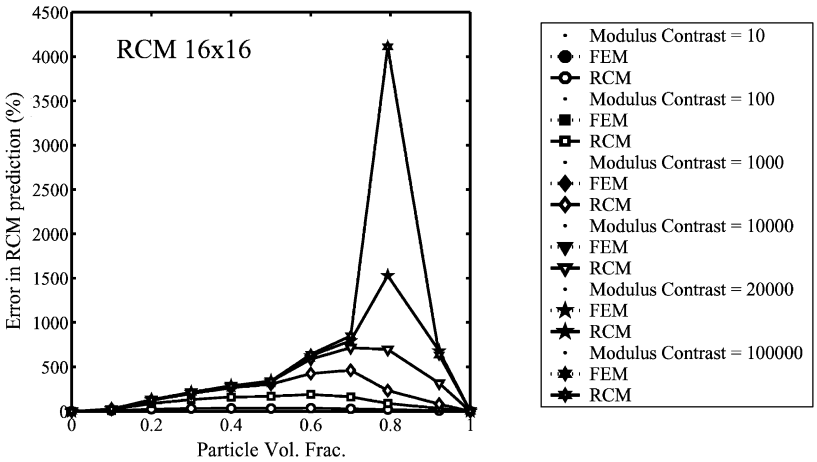

Fig. 6. Error in RCM estimates of Young's modulus with respect to FEM estimates. The smaller RVE (b) has been used for $V_f = 0.80$.

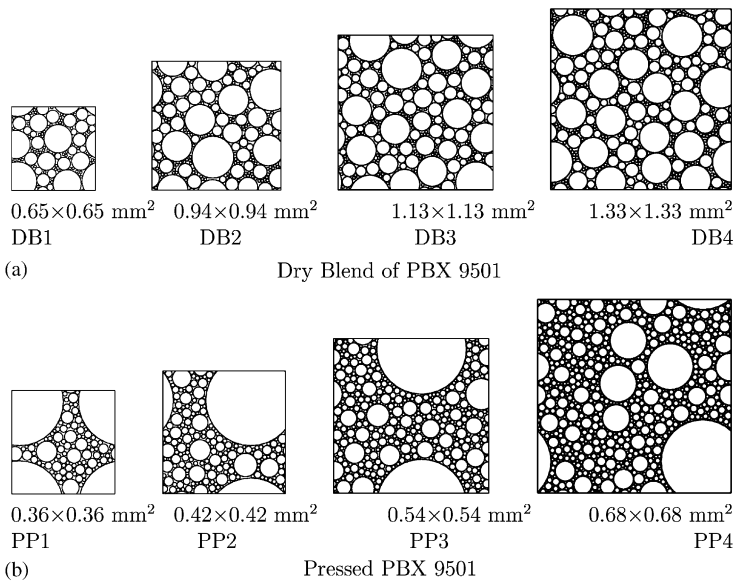

Fig. 7. Microstructures containing circular particles based on the particle size distribution of the dry blend (DB) of PBX 9501 and of pressed (PP) PBX 9501.

20% less than the experimentally determined value of PBX 9501 and therefore a considerable improvement over the estimates discussed previously. However, RCM does not perform as well for the chosen microstructures.

Fig. 4 shows comparisons of FEM and RCM calculations on the models using 256×256 four-noded square elements. RCM tends to overestimate the effective Young's modulus for all volume fractions and modulus contrasts. With increase in the number of subcells in a block, the RCM estimates converge towards the FEM solution. Fig. 5 shows the errors in the RCM estimate with respect to the FEM solution corresponding to the results shown in Fig. 4. If the smaller RVE (b) containing 80% particles is used for the calculations instead of the larger RVE (a) (as shown in Fig. 2), there is an appreciable

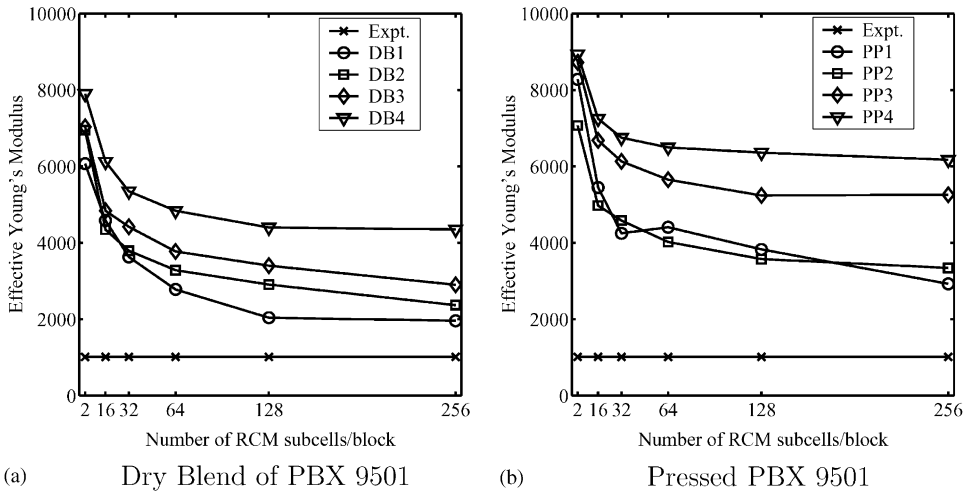

Fig. 8. FEM and RCM predictions PBX 9501. The FEM predictions correspond to the RCM data for 256 subcells/block.

deterioration in the RCM estimates for this volume fraction for the case where 16×16 subcells were used to form each RCM block as shown in Fig. 6. The deterioration is due to the decreased self similarity at different length scales in the smaller RVE containing 80% particles.

Models based on the actual size distribution of PBX 9501 have also been simulated using FEM and RCM. Eight models (shown in Fig. 7), each containing about 86% by volume of particles, were generated and each model was divided into 256×256 square subcells for RCM and FEM calculations. Subcells were assigned HMX properties if they contained more than 50% particles by area. The binder was 'dirty', i.e., effective properties from DEM were assigned to the binder to bring the volume fraction of particles up to 92%. FEM and RCM predictions for these models are shown in Fig. 8. For these microstructures, the FEM estimates of Young's modulus vary from 2 to 6 times the experimental Young's modulus of PBX 9501. Though the RCM estimates are considerably higher than the FEM predictions, these converge to the FEM results with increasing subcells per block. Acceptable accuracy in the RCM approximation is obtained when blocks of 16×16 subcells are used for the RCM calculations for some of the pressed PBX models. However, in other models the error is quite high even when 64×64 subcells are used to model each block.

5. Summary and conclusions

Third-order bounds on effective elastic moduli are too far from the actual moduli of PBX 9501 to be of use. DEM estimates are close to FEM estimates on microstructures without particle–particle contact but underestimate the Young's modulus of PBX 9501. RCM approximations overestimate the effective properties but converge towards FEM estimates with increase in the number of subcells per block. FEM estimates can vary from as low as $\frac{1}{5}$th of the Young's modulus of PBX 9501 to as high as 6 times the modulus depending on the microstructure and the degree of discretization used in model RVEs for the same volume fraction of particles. An appropriately chosen RVE in conjunction with FEM is the best choice for determining the effective moduli of PBX materials among the four methods discussed even though such an approach remains unsatisfactory from a numerical prediction perspective.

Acknowledgements

This research was supported by the University of Utah Center for the Simulation of Accidental Fires and Explosions (C-SAFE), funded by the Department of Energy, Lawrence Livermore National Laboratory, under subcontract B341493.

References

[1] J.M. Zaug, in: Proceedings of the 11th International Detonation Symposium, Snowmass, Colorado, 1998, p. 498.
[2] T.D. Sewell, R. Menikoff, Personal communication, 1999.
[3] C.M. Cady, W.R. Blumenthal, G.T. Gray III, D.J. Idar, in: Proceedings of the International Conference on Fundamental Issues and Applications of Shock-Wave and High-Strain-Rate Phenomena (EXPLOMET 2000), Albuquerque, New Mexico, 2000.
[4] G.T. Gray III, D.J. Idar, W.R. Blumenthal, C.M. Cady, P.D. Peterson, in: Proceedings of the 11th International Detonation Symposium, Snowmass, Colorado, 1998, p. 76.
[5] G.W. Milton, Phys. Rev. Lett. 46 (1981) 542.
[6] K.Z. Markov, in: K.Z. Markov, L. Preziosi (Eds.), Heterogeneous Media: Micromechanics Modeling Methods and Simulations, Birkhauser, Boston, 2000, p. 1.
[7] N. Shah, J.M. Ottino, Chem. Eng. Sci. 41 (1986) 283.